Annals of the Academy of Romanian Scientists
Series on Physics and Chemistry
Online ISSN **2559 – 1061** Volume **9**, Number 1/**2024**

COMPLEX CHARACTERIZATION OF THE BINARY THIN FILMS BASED ON CARBON DEPOSITED BY TVA METHOD

Rodica VLADOIU[1], Aurelia MANDES[2], Virginia DINCA[3], Victor CIUPINA[4], Gabriel PRODAN[5], Vilma BURSIKOVA[6]

Abstract. Metal-carbon (C-Me) thin films with compact structure and extremely smooth surface were prepared using the Thermionic Vacuum Arc (TVA) method in one electron gun configuration, on glass and silicon substrates. The deposited films were further investigated to determine their structure formation, in order to assess their properties and applications. The surface morphology and wettability of the obtained multifunctional thin films were investigated using: Transmission Electron Microscopy (TEM), Scanning Electron Microscopy (SEM) and Free Surface Energy (FSE) by See System. The results from TEM measurements show how the Ag, Mg and Si interacted with carbon and the influence this materials have on the thin film structure formation and the grain size distribution. SEM correlated with EDX (Energy dispersive X ray) results reveal a precise comparative study for understanding the complex nanocrystalline structure with varying features depending on the introduced element (Ag, Si, Mg) and the substrate (Si, SiO2).

Keywords: TVA, Carbides, Nanocrystalline, TEM, SEM, Wettability, Mechanical Properties.

DOI 10.56082/annalsarsciphyschem.2024.1.48

1. Introduction

Modern technology has placed demands for increasing mechanical and chemical capability in materials used for a variety of technological and commercial applications. Both, the number of applications and mechanical/chemical requisitions have grown with a greater rate than the number of materials that can be used to meet them [1-3]. As a result of recent improvement in technologies to see and manipulate the properties of these materials, the nanomaterials field has seen a

[1] Prof. Dr., Faculty of Applied Science and Engineering, Ovidius University, Constanta, Romania, assoc. member of the Academy of Romanian Scientists (e-mail: rvladoiu@univ-ovidius.ro).
[2] Asst. Prof. Dr., Faculty of Applied Science and Engineering, Ovidius University, Constanta, Romania (e-mail: amandes@univ-ovidius.ro) - *Corresponding author.*
[3] Asst. Prof. Dr., Faculty of Applied Science and Engineering, Ovidius University, Constanta, Romania (e-mail: vdinca@univ-ovidius.ro).
[4] Prof. Dr., Faculty of Applied Science and Engineering, Ovidius University, Constanta, Romania, full member of the Academy of Romanian Scientists (e-mail:victorcp41@yahoo.com).
[5] Assoc. Prof. Dr., Faculty of Mechanical, Industrial and Maritime Engineering, Ovidius University, Constanta, Romania (e-mail: gprodan@univ-ovidius.ro).
[6] Assoc. Prof. Dr., Faculty of Science, Masaryk University, Brno, Czech Republic (e-mail: vilmab@physics.muni.cz).

huge increase interest of research community [4, 5].

The properties in turn depend on the atomic structure, composition, microstructure, defects, and interfaces, which are controlled by thermodynamics and kinetics of the synthesis [6, 7]. The optimization of the material combination and deposition parameters is always a challenging subject for each element or combination of elements, especially based on carbon [8].

Nanocrystalline carbon doped thin films gain tremendous potential with excellent properties for technological applications [9-11]. There is a great demand in joining carbon, with other elements such as Ag, Si or Mg, which ensures high resistance against chemical and corrosive environment attack, but, what is of great importance, the better adherence of the carbon on the coated substrates [12].

Ag is a transition metal that possesses the highest electrical conductivity, thermal conductivity, and reflectivity of any metal. Thanks to these properties, silver is used industrially in electrical contacts and conductors, in specialized mirrors, window coatings and in catalysis of chemical reactions. Despite of these facts, pure silver is too soft and expensive to be used. Therefore, by adding silver in carbon matrix, the cost of the thin film will drop and the new material will benefit of enhanced properties [13-17]. Moreover, incorporation of silver results in a decrease of the friction coefficient and improves the wear resistance of carbon materials [18].

Silicon is the principal component of glass, ceramics, for most semiconductor devices intrinsic semiconductor, although the intensity of its semiconduction is highly increased by introducing small quantities of impurities [19-21]. Due to the strong bonding between Si and C, silicon carbide (CSi) films with properties as: high melting point, oxidation resistance, high erosion resistance, high hardness and strength [22-24] are good materials for reactive environment, electronic devices [25] as well as abrasion and cutting applications [26 27]. Also, because of the large band gap (2.2–3.3 eV) is suitable for light emission in the green to blue range [28-31] and silicon carbide materials operates at higher temperatures, voltages, and power than silicon [32].

Magnesium, used as an alloying agent, is one of the elements that improves the mechanical, fabrication and welding characteristics [33]. One of the shortcomings in the Mg thin films is the stress, which is known to have a close correlation not only with the physical properties of the thin films such as mechanical strength, but also with the electrical properties [34, 35]. The use of magnesium in carbon matrix phase is of interest for advanced structural applications and for components in engines with the advantage of high specific strength and stiffness [36-38].

The present paper is considered an overview of the structural and morphological properties of the hydrogen free amorphous carbon films doped with silver, silicon and magnesium using Thermionic Vacuum Arc as the deposition method. Reported in this study are the data for the grain size nanostructures, atomic percentage, elements distribution, spectrum acquisitions and free surface energy evaluation for understanding

the complex nanocrystalline structure with varying features depending on the introduced element (Ag, Si, Mg) and the substrate (Si, SiO2). The direct applications are related to the use of these elements embedded in carbon matrix phase for coating components with high corrosion/wear resistance, high hardness, mechanical strength and good adherence.

2. Experimental set-up

The films with compact structure and extremely smooth surface were prepared using the Thermionic Vacuum Arc (TVA) method in one electron gun configuration [39], on glass and silicon substrates. The cathode consisted of a heated tungsten filament, mounted inside a molybdenum Wehnelt cylinder. The anode was shaped as a crucible, which contained the material to be evaporated, made from mixtures of carbon and silver/silicon/magnesium powders. At a specific value of the high voltage applied between the electrodes, a bright plasma discharge ignited. So, the nature of the flux of particles was a mixed binary plasma of two elements.
Metal nanocrystalline embedded in hydrogen-free amorphous carbon (a-C) matrix samples were prepared following essentially the same technique as described in Ref. [40].
The electrodes were mounted inside a vacuum vessel having a typical residual pressure between $1.0 \cdot 10^{-3}$ Pa→ $1.0 \cdot 10^{-4}$ Pa, while during the process of deposition, the working pressures were: 1.0 Pa for C-Ag plasma, $3.1 \cdot 10^{-1}$ Pa for C-Si plasma and $3.0 \cdot 10^{-1}$ Pa for C-Mg plasma.
Carbon doped thin films were deposited from half percent of binary mixtures of carbon and silver, silicon and magnesium powders, respectively. The parameters for the growth of each of CAg, CMg and CSi thin films are represented by three different set of values, which characterize every step of the deposition: geometrical, plasma ignition and deposition parameters (Table I).

GEOMETRICAL PARAMETERS	PLASMA IGNITION PARAMETERS	DEPOSITION PARAMETERS
• anode – cathode distance (**d_{a-c}**), • anode – holder distance (**d_{a-h}**) • the angle between the cathode and anode vertical axis (**φ**).	• **I_f** - the intensity of the current necessary for the filament heating, • **U_a** – the applied voltage for the ignition • **I_a** – the intensity of the arc current before the breakdown of the plasma.	• the film growth time (**τ**) • the film thickness measured on situ by Cressington thickness monitor (**t_{CMe}**) • work pressure during deposition (**p_{CMe}**) • rate of deposition (**r**).

Table I. Parameters of the thin films deposition

Samples		CAg	CMg	CSi
GEOMETRICAL PARAMETERS				
	d_{a-c} [mm]	5	4	5
	d_{a-h} [mm]	160	170	150
	φ [º]	45	45	45
PLASMA IGNITION PARAMETERS				
	I_f [A]	46.7	43	40
	U_a [V]	$8.1 \cdot 10^2$	$1.0 \cdot 10^3$	$1.8 \cdot 10^3$
	I_a [A]	$3.43 \cdot 10^{-2}$	$1.1 \cdot 10^{-2}$	$6.3 \cdot 10^{-2}$
DEPOSITION PARAMETERS				
	τ[s]	155	60	250
	t_{CMe} [nm]	101	104	107
	p_{CMe} [Torr]	$7.5 \cdot 10^{-3}$	$2.4 \cdot 10^{-3}$	$2.2 \cdot 10^{-3}$
	r [nm/s]	0.65	1.73	0.42

The thin films were deposited on silicon wafers (Si 100) and glass (Gl) substrates, which were previously cleaned in acetone ultrasonic bath for 20 min. We denominated the samples accordingly with the substrates and the material deposited on them as CAg/Si, CSi/Si, CMg/Si for those deposited on silicon wafers and CAg/Gl, CSi/Gl, CMg/Gl respectively for glass substrate. After deposition, prior to any structural or morphological characterization, in order to avoid the oxidation and the physisorbtion, the samples were let to cool down in the deposition chamber for 24 hours.

The surface morphology and wettability of the obtained multifunctional thin films were investigated using: Transmission Electron Microscopy (TEM), Scanning Electron Microscopy (SEM), mechanical properties and Free Surface Energy (FSE) by See System.

3. Results and discussions

Transmission Electron Microscopy (TEM) measurements

In order to analyze the thin films by TEM, the samples were prepared using a simple

method described by Teodorescu et al. [41] using a diamond knife to scratch surface of the film, alcohol as dispersive medium and a 400Cu grid covered by formvar film as support for sample.
Samples were characterized by Transmission Electron Microscopy at 100kV - accelerated voltage. Morphology of samples was evaluated from BFTEM (Bright Field Transmission Electron Microscopy) images and means diameter calculated from experimental data assuming a lognormal distribution for Feret diameters.
Structural features of sample were determined from electron diffraction pattern, using analytical method to index diffraction pattern an Cohen method [42] with modified Nielson-Riley [43] function to accurate determination of lattice parameters. All images were acquired using iTEM platform from Soft-Imaging System connected with MegaView III CCD camera, mounted on Philips CM120ST microscope. Using image-processing future of iTEM platform we select and measure Feret diameters of 100 nanoparticles. In SciDAVIS we build experimental histogram that was fit with lognormal function.
Electron diffraction patterns were acquired at 100kV and 880mm camera length. Using ELD [44] module from CRISP2 [45] the background was fitted with 9th degree polynomial function. Automated procedure implemented in ELD was used to identify peaks, but in addition we applied a manual selection for peak with low intensity. The peak positions were used for indexing diffraction patterns and lattice parameters determination.
The structure of CAg/Gl sample consists in Ag phase and small amount of onion-like carbon [46] (**Figure 1a**). The lattice parameter for Ag phase in this case was 0.412294 nm from analytical method and 0.40593 nm from Cohen method, with relative error compared with [47] of 0.89%, and of 0.66% respectively. The structure of CAg/Si exhibited Si [48] and Ag phase, but also some unknown phase, possible oxide. The lattice parameter in this case was 0.41398nm from analytical method and 0.41391nm from Cohen method, in both cases the relative error was 1.29% [49, 50].
On one of the analyzed areas from the CAg/Gl sample we found only Ag phase (**Figure 1a**). The lattice parameter in this case was 0.411377 nm calculated from analytical method and 0.40869 nm using Cohen method, from diffraction pattern (**Figure 1b,c**). The relative error compared with [51, 52] was 0.6%, and 0.02%respectively. In addition, four very weak peaks have been found and can be assumed that this sample contains Ag2O phase (Figure 2d).

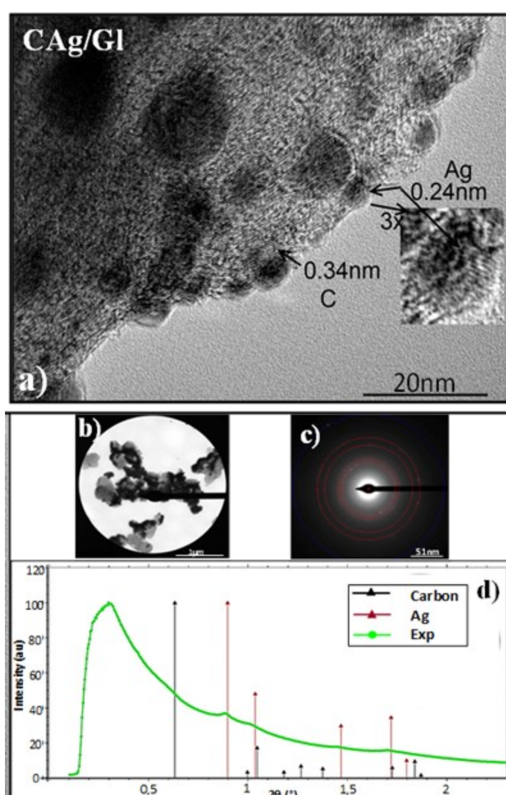

Fig. 1. BFTEM images for CAg, thin films deposited on glass

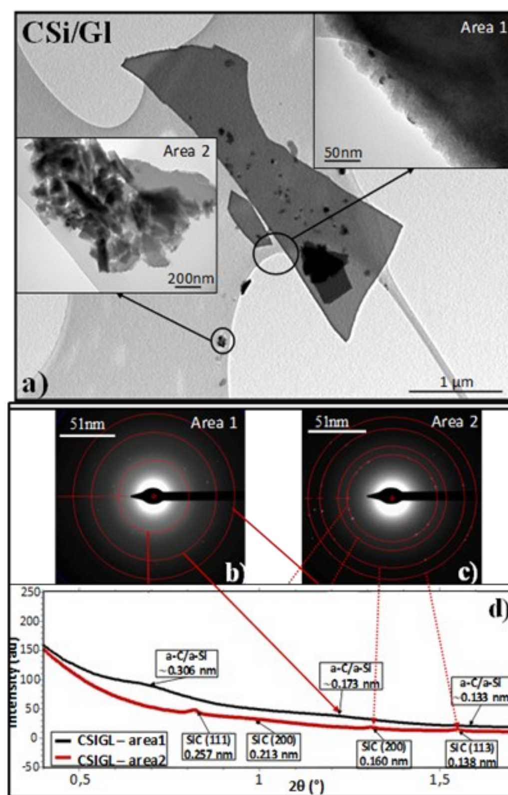

Fig. 2. BFTEM images for SiC, thin films deposited on glass

In the case of CSi/Gl sample, a large piece of film was found on the formvar support, with thickness small enough to identify morphological structure. Insets present the features of sample at higher magnification in two different areas (**Figure 2a**).

Also in **Figure 2b,c** are presented insets of electron diffraction patterns obtained from Area 1 and Area 2. Silicon carbide (SiC) was identified on small aggregate, as we see in diffraction profile extracted using ELD module from CRISP2 application (**Figure 2d**). The identified peak was highlighted to corresponded circle in diffraction pattern. The presence of silicon carbide in CSi/Si is very low, ELD identified only (111) peak of SiC. The SiC lines was indexed using cubic phase (F4-3m, a=0,4348nm) [46, 48]. Structural, the C-Mg/Gl film (**Figure 3a, b,c**) consists of small peaks that belong to the hexagonal structure of Mg (P 6(3)/mmc, a = 0.32095Å, c = 0.52104Å [44]). In the case of the CMg/Si thin film next to the hexagonal structure of Mg cubic structures of MgO (Fm3m, a=4.2170Å), MgO was also found [46, 50].

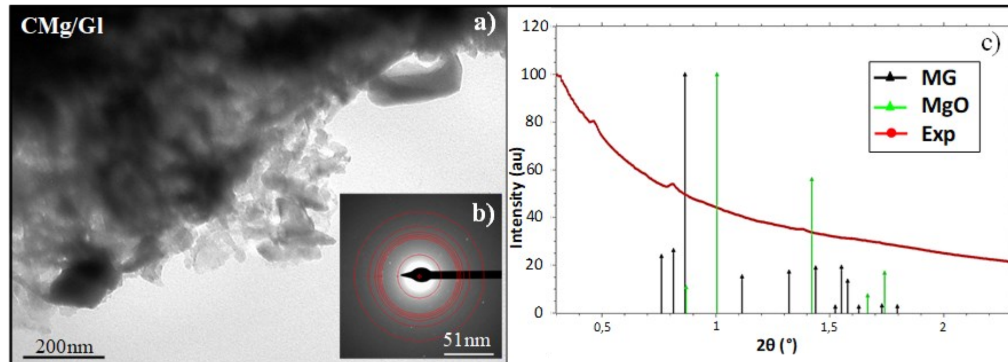

Fig. 3. BFTEM images for CMg thin films deposited on glass

The particle size histograms were drawn from the TEM micrographs, resulting the mean size of the particles. It is well-known that the crystallites dimension depends on the nature of the substrate. **Figure 4** shows the particle size distribution of CAg, CSi and CMg nanoparticles on glass substrate, it can be seen that in the case of CMg/Gl the particle sizes possess a small and narrow size distribution in a range from 15 to 55 nm, and the mean diameter is about 30.8 nm.

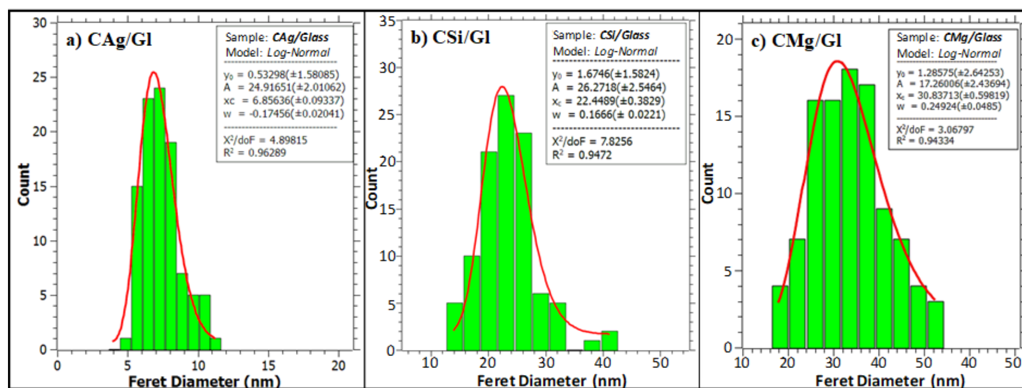

Fig. 4. Grain size distribution graphs for CAg, CSi, CMg films on glass substrate

For CAg/Gl (**Figure 4a**) the maximum frequency of mean diameter was xc = 6.85 nm, while for CSi/Gl (**Figure 4b**) the histogram reveals the mean diameter of xc = 22.44 nm. These differences provides specific behaviors for mechanical properties.

From the morphological point of view, the CMg/Gl deposited film does not have a uniform structure, being a nonregular shape of nanoparticles, with the average dimension of 30.83 nm (**Figure 4c**). For the CMg/Si sample the film is well crystalized as polycrystalline structure with grains of approximately 90 nm.

Scanning Electron Microscopy (SEM)

SEM images were performed using a Scanning electron microscope EVO 50 XVP (Carl Zeiss NTS) with EDX attachment (Bruker). Based on the SEM images, the equipment can generate characteristic X-ray, secondary and back-scattered electrons. EDX measurements were carried out with a Bruker accessory fitted on the Zeiss Evo 50 scanning electron microscope. It is well known that EDX quantitative analysis has limitations, specifically when determining the quantitative atomic composition of a given material. Depending on specific conditions (applied voltage, atomic structure, etc.) the light elements with atomic number $Z < 11$ cannot be routinely and accurately analyzed using EDX. This concerns Carbon, as well. However, taking into account that TVA method assures high purity for the deposited thin films, and other elements were not identified as impurities, one can be confident on these results.

The atomic concentration ratio deduced from SEM for the MeC thin films are presented in **Table II**.

Table II. Atomic concentration ratio deduced from SEM for the C-Me thin films on Si substrate

Elements	CAg	CSi	CMg
C	24.68 %	7.48 %	21.23 %
Si	35.56 %	87.47 %	-
O	6.98 %	5.05 %	5.76 %
Ag	2.78 %	-	-
Mg	-	-	73.01 %

The technique of Scanning Electron Microscopy (SEM) was employed extensively throughout this study to examine images of both the surface morphology and EDS mappings of the deposited elements on samples of silicon. The SEM images of the films show smooth, uniform surface without cracks and well covered to the substrate (**Figure 5**).

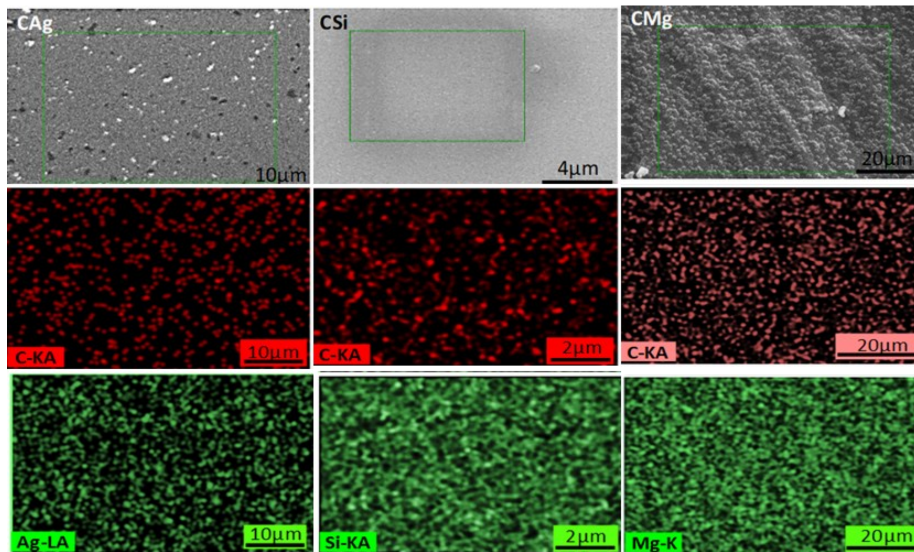

Fig. 5. Scanning Electron Microscopy captures and mapping for CAg, CSi, CMg films on Si substrate

Mechanical properties of C-Ag films

The indentation resistance of the C-Ag films deposited on glass and silicon substrates was studied using several different indentation techniques. The first set of measurements was carried out using quasistatic nanoindentations with 20 unloading segments. The time dependence of the indentation load and an example of the resulting displacement obtained during indentation testing of C-Ag film deposited on silicon substrate is illustrated in **Figure 6**.

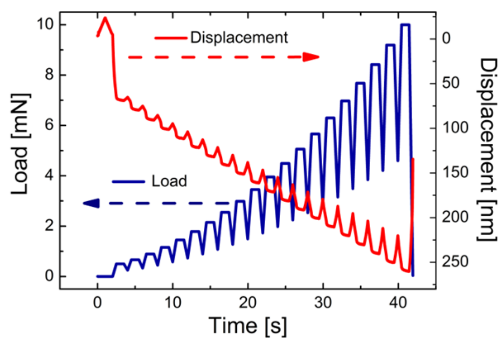

Fig. 6. Time dependence of the load during the quasistatic nanoindentation test with 20 unloading segments and an example of the resulting displacement carried out on C-Ag/Si sample.

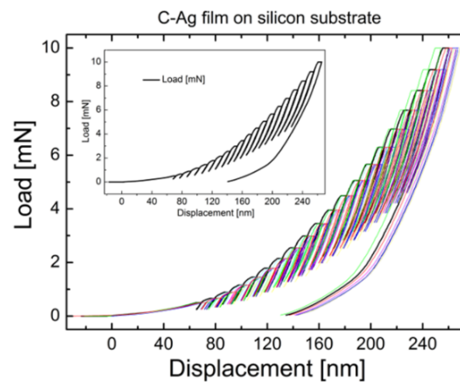

Fig. 7. Loading curves with 20 unloading segments obtained on C-Ag/Si films deposited on silicon substrate - C-Ag on single crystalline silicon substrate. Each color represents an individual measurement at a different place on the sample.

The quasistatic loading curves with 20 unloading segments shown in **Figure 7** were obtained at eight different places on the C-Ag film deposited on a single crystalline silicon substrate. Each color represents an individual measurement at a different place on the sample. The curves obtained from different places show only a slight scatter. Each of the unloading segments was analyzed according to Oliver and Pharr approach in order to get dependence of the hardness and reduced elastic modulus from the near surface of the C-Ag film up to the film substrate interface. The last (20th) unloading segments in **Figure 7** exhibit an elbow, which is characteristic of unloading response of single crystalline silicon, and it is formed due to pressure-induced phase transformation. According to this effect, it is possible to recognize when the influence of the substrate on the measured nanoindentation data starts to predominate.

Similar curves were obtained on a glass substrate, the depth profiles of hardness and effective elastic modulus obtained at different places are shown for C-Ag/Si and C-Ag/Gl samples in **Figure 8**. According to these results, it is possible to affirm that the data are well reproducible for the samples set.

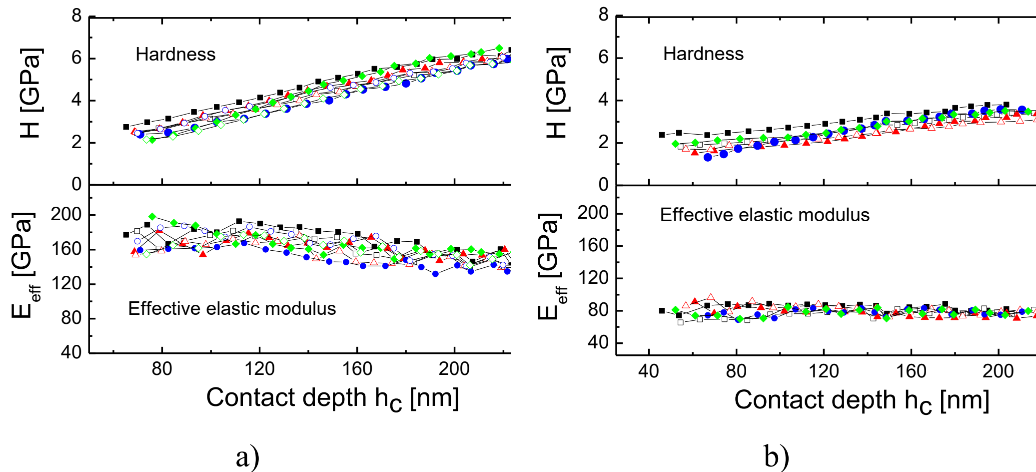

Fig. 8. Dependences of the hardness and effective elastic modulus (calculated according to equation 2) on contact depth **C-Ag/Si (a)** and **C-Ag/Gl (b)**.
Measurements at different places on the sample are distinguished with a different color.

The comparison of the average hardness and effective modulus values dependent on the indentation depth is presented in **Figure 9**. It is shown that the average hardness values gradually increase with the contact depth hc. The hardness results approach 2 and 1.8 GPa for contact depths below 40 nm as it can be seen in **Figure 9**. Although the structures of Ag/Si and C-Ag/Gl samples are very similar, there is, at first sight, a large difference in the effective elastic modulus profile for samples deposited on silicon and glass substrates. In the case of C-Ag/Si, there is a drop in

elastic modulus values at about 155 nm, suggesting the start of the substrate influence. This fact is very curious because the influence of the substrate hardness on the measured values of the hardness is starting at indentation depths around 50 nm; therefore, the substrate influence on elastic modulus data should start at much lower depths as in the case of the hardness. Thus, the effective elastic modulus of C-Ag/Si sample appears as high as 180 GPa because the elastic modulus data for the depth around 40 GPa is fully influenced by the silicon substrate effective modulus, which for low loads is also around 180 GPa. The drop in E_{eff} values at about 160 nm was probably caused by the well-known pressure-induced transformation of the single crystalline silicon.

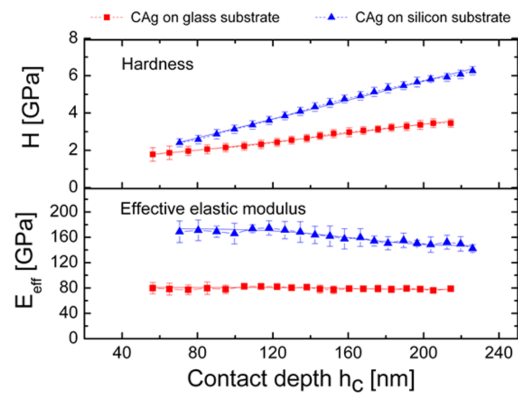

Fig.9. The comparison of the averaged hardness and effective modulus values depending on the indentation depth

The elastic modulus values were measured by a nanodynamical mechanical analysis using the modulus mapping capability. During the in-situ imaging process, the system continuously monitors the dynamic response of the sample to the oscillating load as a function of the position.

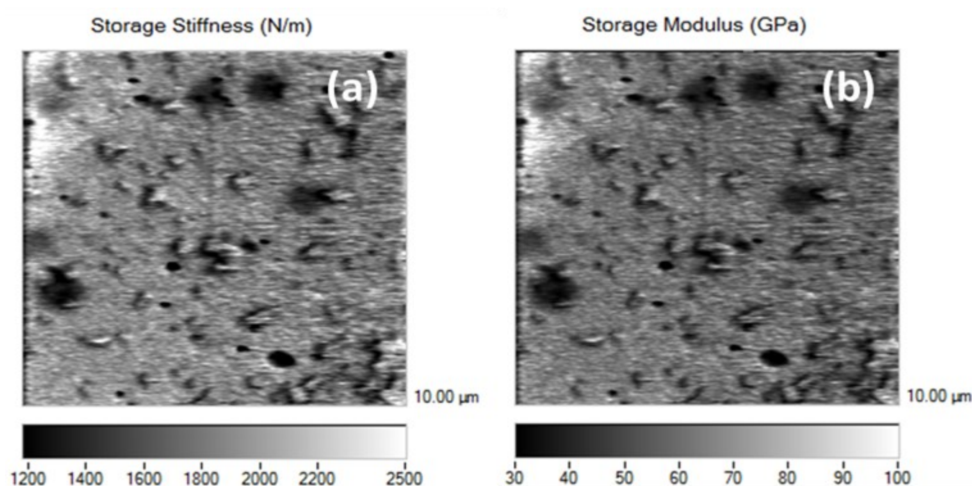

Fig. 10. Quantitative maps of the storage stiffness a) and the storage modulus b) obtained on C-Ag/Si surface.

Therefore, at each image pixel (256×256 pixels), the storage and loss stiffness and the storage and loss moduli values are determined. Quantitative maps of the storage stiffness and the storage modulus (**Figure 10**) were carried out at a frequency of 300 Hz with Cube Corner indenter. The oscillating force amplitude was 1 μN, the oscillation frequency was 300 Hz and the displacement amplitude was around 1 nm. The results confirmed our previous assumptions about the influence of the silicon substrate on the measured data. It was shown that the modulus values are similar to those obtained on a glass substrate. Moreover, it was possible to visualise the local changes in the modulus and stiffness showing that the coatings contain Ag particle aggregates with elastic response different from the matrix.

The same effect of spontaneous Ag particle aggregation on the sample surface and in the near-surface region of the Ag-C films was reported in [37]. The aggregation process was accentuated during the in situ scanning with a contact force of 2 μN and also during the indentation tests. A similar effect was observed for wear tests in [38]. This particle agglomeration may be the reason for the low surface hardness values reached compared to the pure carbon films prepared using TVA method [39].

Free surface energy (FSE)

Materials wettability is a characteristic parameter that influences surface related processes such as adhesion [53], and can be calculated by contact angle method. Determination of the contact angle, enables estimation of the type of interaction between surfaces and liquids (dispersive and polar interactions) [54]. It helps to

predict the course of reaction during the chemical processing of surfaces in a liquid environment (washing, dyeing), as well as when producing good mechanically resistant composite materials.

The calculus was performed by using the See System computer software [55] that uses the measurement of the tangent angle of a sessile liquid drop on a solid surface. For each sample distilled water and formamide were used as testing liquids and the obtained value represents the average of ten measurements recorded over an extended area of the surface at the room temperature (25◦C). In **Figure 11** are presented the pictures of the drops captured during the contact angle measurements on the three different samples (SiC/Silicon, SiC/Glass and SiC/OLC45).

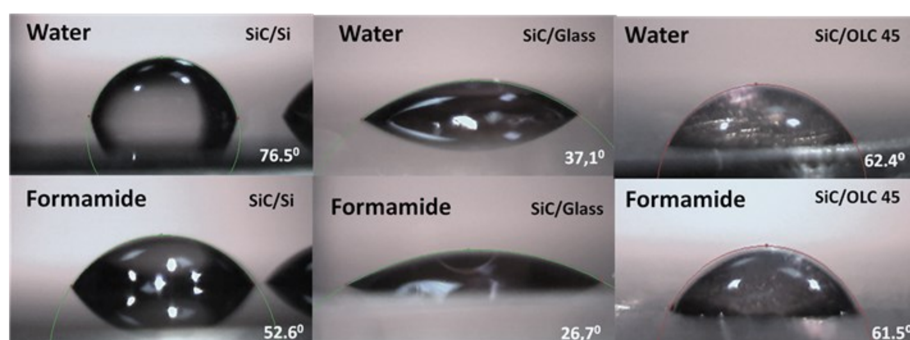

Fig. 11. Photos of the droplets on Si/ Glass/ OLC 45 sample

The surface wettability changes were followed by contact angle measurements. The droplets volume was set to 4µl for all experiments and the surface free energy was evaluated by using equations of states mathematical formulas models as: Kwok-Neumann model, Li-Neumann model and Wu model.
The corresponding evaluated surface energies of distilled water (θ_w) and formamide (θ_f) are shown in **Table III**.

Table III. Comparison between the SFE's in different models of evaluation

Samples	*Surface free energy γ [mJ/m²]*		
	Kwok-Neumann	*Li-Neumann*	*Wu-eq. of state*
SiC/Si	38.67	39.10	37.67
SiC/Glass	56.42	52.10	58.47
SiC/OLC45	40.03	40.40	38.97

As a sensitive indicator of changes in the level of surface energy and changes in the chemical and super-molecular structure of the surfaces to be modified, the contact angle measurements have shown reproducible results ranging from 37.610 to 76.620 for water and 26.530 to 61.420 for formamide. These results were obtained

for the group of samples deposited on silicon wafer, glass and stainless steel OLC 45 substrates under the deposition conditions presented in Table III. The highest surface free energy, among the tested samples, was obtained in the case of CSi/Glass sample (58.57mJ/m2), while the lowest for CSi/Si sample (39.03 mJ/m2). It can be noticed that the use of different substrates materials has a reduction of the surface free energy in two cases (out of three tested).
At the first view, the obtained values are very close to the ones obtained for SiC and Si films on Si substrate. The difference between the results obtained in this study and the ones from the reference mentioned above is a consequence of the experimental parameters variation, such as gas pressure and the distance between the plasma discharge and the holder of samples.

Conclusions

From the TEM measurements, the CAg/Glass sample consists in Ag phase with Ag nanoparticles of 6.85 nm diameter and onion like – carbon [C] with diameter of 159.61. In the case of CAg/Si, the diameter of Ag nanoparticles was 23.20 nm. The CMg films presents crystalline structure, with hexagonal Mg for CMg/Si and cubic phase for CMg/Gl. Both deposition are nanostructured, with average grain size of 30 nm for CMg/Gl, respective 55 nm for CMg/Si. For CSi films we find out an amorphous form of C revealing the presence of crystalline zones identified as cubic SiC structure.

The Surface Free Energy reveals hydrophilic properties correlated to the topography, but also with the composition of the film, with values of approximately 40 mJ/ m2. In this way, the study the structural and morphological properties of the hydrogen free amorphous carbon films doped with Ag, Si and Mg by Thermionic Vacuum Arc method would promote applications related to the use of these combinations for coating components with requested defined wettability and high corrosion/wear resistance, generated by specific grain sizes.

REFERENCES

[1] W. Daves, A. Krauss, V. Haublein, A. J. Bauer, L. Frey, Mat. Sci. Forum 717-720 (2012) 1089-1092.
[2] H. Jian-Feng, Z. Xie-Rong, L. He-Jun, X. Xin-Bo, H. Min, Carbon 41 (2003) 2825-2829.
[3] H.X. Zhang, P.X. Feng, V. Makarov, B.R. Weiner, G. Morell, Mat. Res. Bull. 44 (2009) 184–188
[4] Q. W. Huang, L. H. Zhu, Mater. Lett. 59 (2005) 1732– 1735.
[5] L. Lianbi, C. Zhiming, X. Longfei, Y. Chen, Mater. Lett. 93 (2013) 330–332.
[6] Z.Wang, S. Wang, C. Zhang, J. Li, J. Nanopart. Res. 13 (2011) 185–191.
[7] H. Jafari, N. Ehsani, S. A. Khalifeh-Soltani, M. Jalaly, Appl. Surf. Sci. 264 (2013) 128-132.
[8] S. Meng, D. H. Wang, G. Q. Jin, Y. Y. Wang, X. Y. Guo, Mater. Lett. 64 (2010) 2731–2734.

[9] Saswata Bose, Tapas Kuila, Ananta Kumar Mishra, R. Rajasekar, Nam Hoon Kim, Joongm Hee Lee, , J. Mater. Chem., 22 (2012) 767-784
[10] Yu Zhou, Huajun Guo, Yong Yang, Zhixing Wang, Xinhai Li, Rong Zhou, Wenjie Peng, , Materials Letters, 168 (2016) 138-142, ISSN 0167-577X
[11] B.-F. Hsieh, S.T. Chang, M.H. Lee, , Thin Solid Films, 529 (2013) 444-448, ISSN 0040-6090
[12] Y. Li, J.P. Tu, , D.Q. Shi, X.H. Huang, H.M. Wu, Y.F. Yuan, X.B. Zhao, , Journal of Alloys and Compounds, 436, 1–2 (2007) 290–293
[13] Michael Shincheon Jeea, Hyo Sang Jeona, Cheonghee Kim, Hangil Lee, Jai Hyun Koh, Jinhan Cho, Byoung Koun Min, Yun Jeong Hwang, , Applied Catalysis B:Environmental, 180 (2016) 372–378
[14] Hüseyin Göktepe, Halil Şahanb, Şaban Patat, (2016) doi:10.1016/j.ijhydene.2016.03.074
[15] Hamid R. Lotfi Zadeh Zhad, Rebecca Y. Lai, , Analytica Chimica Acta, 892 (2015) 153–159
[16] Paulo A. Raymundo-Pereira, Anderson M. Campos, Thiago M. Prado, Leonardo N. Furini, Naiza V. Boas, Marcelo L. Calegaro, Sergio A.S. Machado, , Analytica Chimica Acta, 926 (2016) 88–98
[17] Sunna Hwang, Sun Young Noh, Heesuk Kim, Min Park, Hyunjung Lee, , Thin Solid Films, 562 (2014) 445-450, ISSN 0040-6090
[18] M.M. Klak, G. Zatryb, J. Wojcik, J. Misiewicz, P. Mascher, A. Podhorodecki, Thin Solid Films, 611 (2016) 62-67, ISSN 0040-6090
[19] Run-Ning Zhao, Ju-Guang Han, Yuhua Duan, Thin Solid Films, 556 (2014) 571-579, ISSN 0040-6090
[20] Shuai Zhang, Chang Geng Luo, Hua Yang Li, Cheng Lu, Gen Quan Li, Zhi Wen Lu, Materials Chemistry and Physics, 160 (2015) 227-236, ISSN 0254-0584
[21] W. Daves, A. Krauss, N. Behnel, V. Häublein, A. Bauer, L. Frey, Thin Solid Films, 519, 18 (2011) 5892- 5898, ISSN 0040-6090
[22] A.V. Vasin, Sh. Muto, Yu. Ishikawa, A.V. Rusavsky, T. Kimura, V.S. Lysenko, A.N.Nazarov, Thin Solid Films, 519, 7 (2011) 2218-2224, ISSN 0040-6090
[23] A.K Costa, S.S Camargo Jr, C.A Achete, R Carius, Thin Solid Films, 377–378 (2000) 243-248, ISSN 0040-6090
[24] Swarnima Singh, M. Sribalaji, Nitin P. Wasekar, Srikant Joshi, G. Sundararajan, Raghuvir Singh, Anup Kumar Keshri, , Applied Surface Science, 364 (2016) 264-272, ISSN 0169-4332
[25] J. Yun, J. Huang, A. Teal, K. Kim, S. Varlamov, M.A. Green, Thin Solid Films, 609 (2016) 12-18, ISSN 0040-6090
[26] K.-D. Bouzakis, E. Bouzakis, S. Kombogiannis, R. Paraskevopoulou, G. Skordaris, S. Makrimallakis, G. Katirtzoglou, M. Pappa, S. Gerardis, R. M'Saoubi, J.M. Andersson, Surface and Coatings Technology, 237 (2013) 379-389, ISSN 0257- 8972
[27] Javier Llorente, Benito Román-Manso, Pilar Miranzo, Manuel Belmonte, , Journal of the European Ceramic Society, 36, 3 (2016) 429-435, ISSN 0955-2219
[28] B. Swatowska, S. Kluska, M. Jurzecka-Szymacha, T. Stapinski, K. Tkacz-Smiech, Applied Surface Science 371 (2016) 91–95
[29] R.M.S. dos Reis, R.L. Maltez, E.C. Moreira, Y.P. Dias, H. Boudinov, Applied Surface Science 258 (2012) 7395– 7400
[30] A.V. Vasin, Sh. Muto, Yu. Ishikawa, J. Salonen, A.N. Nazarov, V.S. Lysenko, Thin Solid Films, 519, 12 (2011) 4008-4011, ISSN 0040-6090
[31] C. Buttay, D. Planson, B. Allard, D. Bergogne, P. Bevilacqua, C. Joubert, M. Lazar, C. Martin, H. Morel, D. Tournier, C. Raynaud, Materials Science and Engineering: B, 176, 4 (2011) 283-288, ISSN 0921-5107
[32] Iu Kogut, M.-C. Record, Thin Solid Films, 522 (2012) 149-158, ISSN 0040-6090

[33] Li-jun He, Li-yan Wang, Wei-Zhong Chen, Xing-zhao Liu, Journal of Alloys and Compounds, Volume 679 (2016) 122-124, ISSN 0925-8388
[34] Jun-Seong Lee, Jae-Hun Kim, Sang Sub Kim, Thin Solid Films, 595, A (2015) 148-152, ISSN 0040-6090
[35] F. Reischer, E. Pippel, J. Woltersdorf, S. Stöckel, G. Marx, Materials Chemistry and Physics, 104 1 (2007) 83-87, ISSN 0254-0584
[36] W. Hufenbach, M. Andrich, A. Langkamp, A. Czulak, Journal of Materials Processing Technology, 175, 1–3 (2006) 218-224, ISSN 0924-0136
[37] Musa, G.; Mustata, I.; Blideran, M.; Ciupina, V., Vladoiu, R.; Prodan, G.; Vasile, E.; Ehrich, H.. Acta Phys. Slovaca 2005, 55, 417–421.
[38] A. Mandes, R. Vladoiu, V. Dinca, G. Prodan, 42, 10 (2014) 2806 – 2807, ISSN 0093-3813
[39] R. Vladoiu, G. Musa, I. Mustata, Journal of Optoelectronics and Advanced Materials, 5, 1 (2003) 325 – 330
[40] R. Vladoiu, A. Mandes, V. Dinca Balan, G. Prodan, P. Kudrna and M. Tichý, Plasma Sources Science and Technology, 24, 3 (2015)
[41] V.S. Teodorescu, M-G. Blanchin, Microsc. Microanal. 15 (2009)
[42] J. I. Langford, "J. Appl. Cryst. 6 (1973)190
[43] H. Lipson, University College Cardiff Press, 1984
[44] Zou, X.D., Sukharev, Y. and Hovmöller, S., Ultramicroscopy 52 (1993) 436-444
[45] Hovmöller, „S. CRISP: crystallographic image processing on a personal computer" Ultramicroscopy 41 (1992) 121-135
[46] WWW-MINCRYST, GRAPHITE-1800
[47] WWW-MINCRYST, SILVER-4219
[48] WWW-MINCRYST, SILICON-4221
[49] Wyckoff R.W.G.Crystal Structures, 1, 108-110, (1963
[50] WWW-MINCRYST, MAGNESIUM-2671
[51] WWW-MINCRYST, PERICLASE-3533
[52] Kock-Yee Law, Hong Zhao, Springer International Publishing Switzerland (2016) ISBN 978-3-319-25214-8
[53] V. Bursikova, P. St'ahel, Z. Navratil, J. Bursik, J. Janca, Masaryk University Brno, 2004, ISBN80-210-3563-3
[54] R. Vladoiu, V. Dinca, G. Musa, Eur. Phys. J. D 54 (2009) 433–437, DOI: 10.1140/epjd/e2009-00178-5
[55] S. Siboni, C. Della Volope, D. Maniglio, M. J. Brugnara, Colloid and Interface Sci. 271 (2004) 454-472.